

*Supplementary Information for:*

**Cu site differentiation in tetracopper(I) sulfide clusters enables biomimetic N<sub>2</sub>O reduction**

Pinar Alayoglu<sup>†</sup>, Suresh C. Rathnayaka<sup>†</sup>, Tieyan Chang<sup>‡</sup>, SuYin Grass Wang<sup>‡</sup>, Yu-Sheng Chen<sup>‡</sup> and Neal P. Mankad<sup>†\*</sup>

<sup>†</sup>Department of Chemistry, University of Illinois at Chicago, Chicago, IL 60607, USA

<sup>‡</sup>ChemMatCARS, The University of Chicago, Argonne, IL 60439, USA

\*E-mail: [npm@uic.edu](mailto:npm@uic.edu)

## General Synthetic Considerations

All air sensitive reactions were conducted in a MBraun glovebox under nitrogen atmosphere. Reagents were purchased from commercial vendors unless otherwise noted. Reaction solvents were purchased from commercial vendors, dried using a Solvent Purification System (Innovative Technology or Pure Process Technology),<sup>1</sup> then stored over freshly activated 5-Å molecular sieves prior to use. Deuterated solvents were purchased from Cambridge Isotope Laboratories (Tewksbury, MA) and were dried and then stored over freshly activated 5-Å molecular sieves prior to use. NMR spectra were collected on a Bruker DPX 400 NMR spectrometer (400 MHz <sup>1</sup>H). Chemical shifts in  $\delta$  (ppm) were referenced to the solvent residual peak for <sup>1</sup>H NMR and to an external phosphoric acid sample ( $\delta = 0$ ) for <sup>31</sup>P NMR. NMR data were phased, background subtracted or corrected, and integrated using MestReNova version 8.1.

## Synthetic Procedures

Literature procedures were used to synthesize and obtain X-ray quality crystals of [Cu<sub>4</sub>( $\mu_4$ -S)(dppm)<sub>4</sub>][PF<sub>6</sub>]<sub>2</sub> (**1**),<sup>2</sup> [Cu<sub>4</sub>( $\mu_4$ -S)(dppa)<sub>4</sub>][PF<sub>6</sub>]<sub>2</sub> (**2**),<sup>3</sup> and [Cu<sub>2</sub>(dppa)<sub>2</sub>][PF<sub>6</sub>]<sub>2</sub> (**3**).<sup>4</sup>

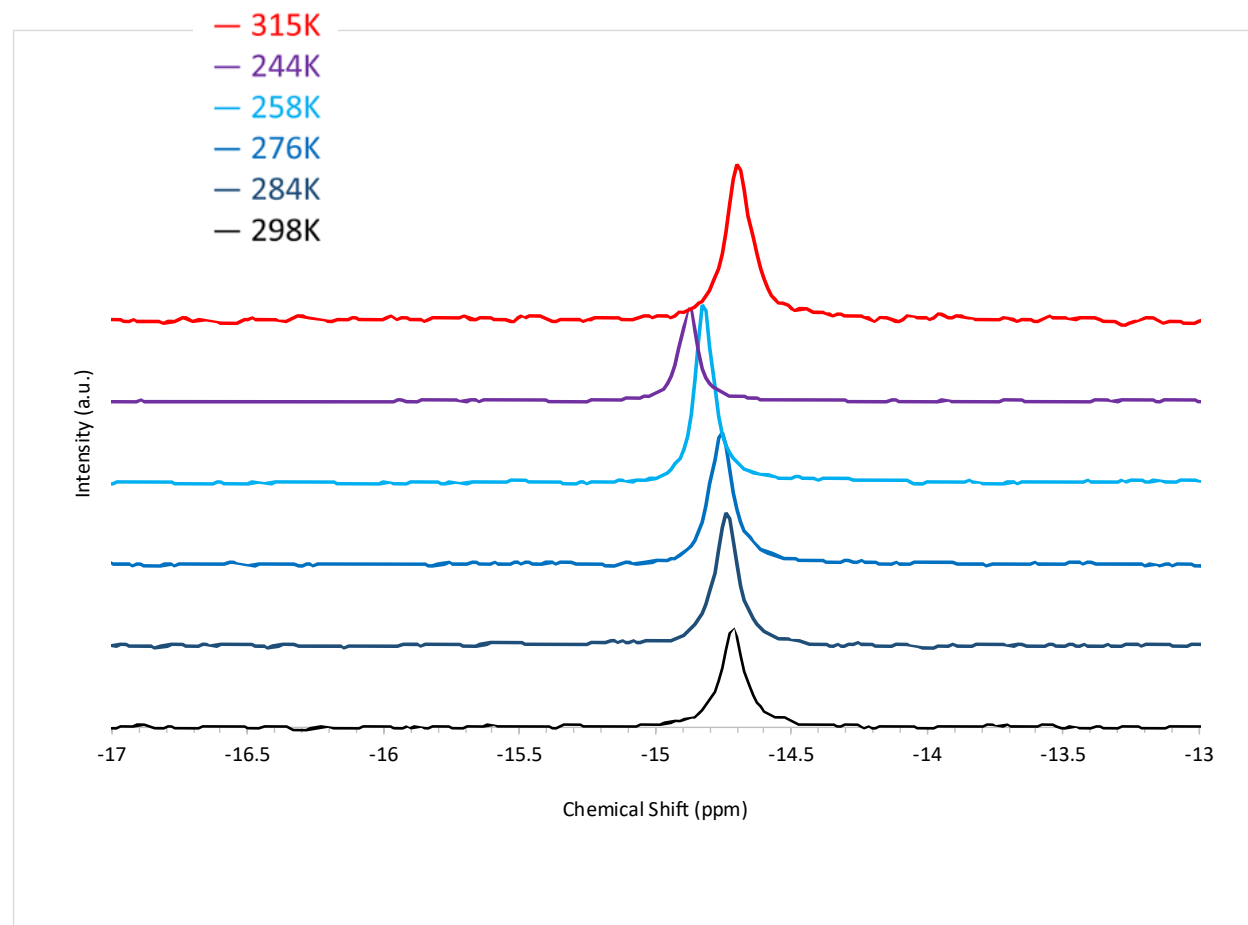


Figure S1. <sup>31</sup>P{<sup>1</sup>H} NMR spectra of **1** in methanol-*d*<sub>4</sub> over the temperature range 244–315 K.

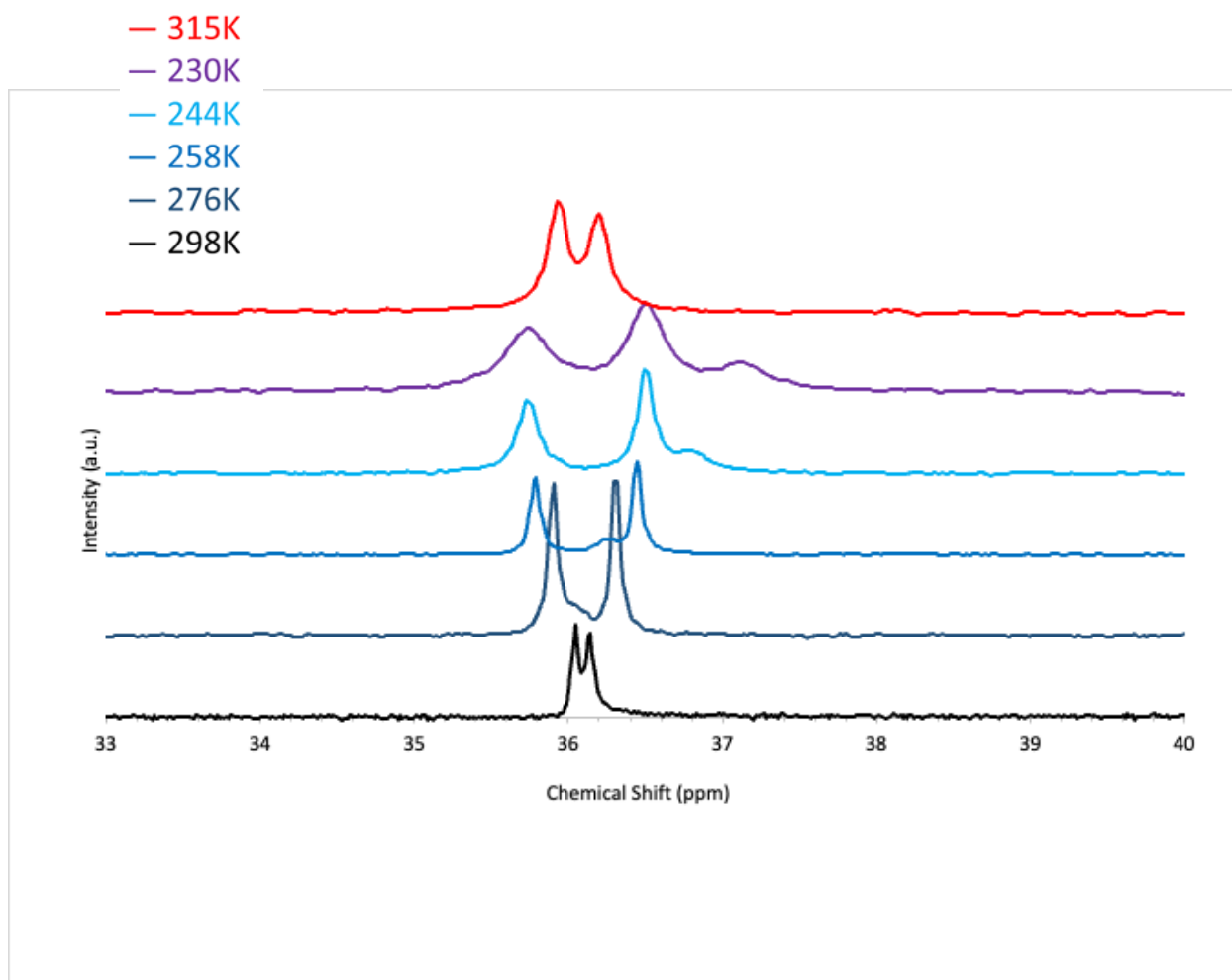


Figure S2.  $^{31}\text{P}\{^1\text{H}\}$  NMR spectrum of **2** in  $\text{methanol-}d_4$  over the temperature range 244-315 K.

## X-ray Diffraction Data Collection

Single crystal X-ray diffraction experiments were performed at NSF's ChemMatCARS (Sector 15) of the Advanced Photon Source (APS), Argonne National Laboratory (ANL). The following procedure described for  $[\text{Cu}_4\text{S}(\text{dppm})_4][\text{PF}_6]_2$  (**1**) is applicable to all the crystals studied.

A yellow plate with dimension  $100 \times 90 \times 80 \mu\text{m}^3$  was mounted on a  $5\text{-}\mu\text{m}$  diameter fiber tip with paratone oil and cooled down to 77.15 K with an Oxford Cryojet. The beam energy was 30 keV ( $0.41328\text{\AA}$ ), and the beam size at the sample was  $0.1 \times 0.1 \text{ mm}^2$  to screen the crystal. After the high quality of the crystal was verified, a complete data set was collected for precise structure determination.

Data were collected using a Huber 3 circles diffractometer with a kappa angle offset of  $60^\circ$  and equipped with a Pilatus3X 2M(Si 1mm) detector. The distance between the detector and the crystal was 150 mm. A total of 1440 frames were collected at two  $\theta$ -angles sitting at  $0^\circ$  followed by two different  $\omega$ -angles =  $-180^\circ$ ; Kappa =  $0^\circ$  and  $\omega$ -angles =  $-180^\circ$ ; Kappa =  $30^\circ$ , respectively. The data was collected with the  $\phi$ -the angle scanned over the range of  $360^\circ$  with  $0.5^\circ$  scan width using shutterless mode.

Pilatus standard *CBF* frames were collected using a user-friendly data collection software; simultaneously, the *CBF* frames were converted to Bruker's *sfrm* format to perform the data integration using the Bruker APEX II suite software. Data reduction was conducted with SAINT v.8.32B and SADABS v.2013 programs included in the APEX II suite.

The structure solution and refinement were carried out with SHELX software using the XPREP utility for the space group determination and the XT and XL programs for the structure solution and the structure refinement, respectively.<sup>5,6</sup> In addition to this, some structures were solved and refined using SHELXS/SHELXL programs within the Olex2 crystallographic package.<sup>7</sup> The final models from 30-keV data used for DAFS refinement below are available for download from the CCDC (deposition numbers 2293203-2293205). These structures closely match the literature precedents cited above.

Table S1. Crystal dimensions.

Crystal	Dimensions ( $\mu\text{m}^3$ )
$[\text{Cu}_4\text{S}(\text{dppm})_4][\text{PF}_6]_2$ ( <b>1</b> )	100 x 90 x 80
$[\text{Cu}_4\text{S}(\text{dppa})_4][\text{PF}_6]_2$ ( <b>2</b> )	100 x 100 x 80
$[\text{Cu}_2(\text{dppa})_2][\text{PF}_6]_2$ ( <b>3</b> )	100 x 100 x 80

## X-ray Anomalous Diffraction Fine Structure (DAFS)

At the vicinity of the K-edge of the absorbing metal, the imaginary ( $f''$ ) and the real ( $f'$ ) components of atomic scattering factor show substantial changes. DAFS experiments exploit these significant variations at around the near (K-) edge of absorbing metal. To achieve this, single crystal diffraction patterns are collected at the proximity of the K-edge and fitted to refine the  $f''$  and  $f'$  terms of the scattering factor (eq. 1) for the absorber metal for each crystallographically unique atomic site in each crystal lattice, while the scattering factors of all other scatterers are held constant<sup>10</sup>.

$$f = f_0 + f' + if'' \quad (\text{eq. 1})$$

The DAFS experiments were carried out in three stages for each sample:

- First, a complete X-ray diffraction data set was collected at 30 keV (see above). This 30 keV data set was integrated, scaled, and refined to obtain the lattice parameters, atomic coordinates, and thermal parameters that served as the structural model for the subsequent DAFS datasets.
- Second, an X-ray fluorescence scan was obtained at the Cu K-edge using the fluorescence Votex detector scan at  $\pm 50$  eV of the edge in 1-eV intervals to decide the energies to be selected for partial diffraction (i.e., DAFS) datasets.
- Third, based on the XRF spectrum, DAFS data were collected at 5 eV, 1-2 eV, and 3 eV increments before, in, and after the K-edge jump, respectively. DAFS data collection strategy for each energy was compiled based on crystal symmetry. The data collection strategy was chosen to keep the data/parameter ratio  $> 100$  in the  $f'$  and  $f''$  refinement.

### DAFS Data Processing

Upon indexing, integration, and scaling of the reflections from the DAFS datasets, data processing was carried out employing JANA2006<sup>8</sup> following literature procedures.<sup>9,10</sup> The  $f''$  and  $f'$  scattering factors for each crystallographically unique Cu site were freely refined and fitted to the model structure obtained by the refinement of 30-keV data. All pairwise distances were evaluated, and the structure factor, shown in complex form in eq. 1, was extracted for each crystallographically unique Cu atom. Cu K-edge X-ray absorption spectrum, in fluorescence yield mode, from a high purity Cu foil was employed for energy calibration. Athena software<sup>11</sup> was used for background reduction, intensity normalization and energy correction. The Cu K-edge position was taken as 8979 eV. The energy correction was applied to the DAFS plots as well as the X-ray absorption spectra.

During initial qualitative analysis, the energy values for  $f'_{\text{falling}}$  and  $f'_{\text{rising}}$  were estimated by noting where the traces crossed half-maximum amplitude in the falling and rising edge regions, respectively. A more detailed procedure for determination of  $f'_{\text{rising}}$  used in linear regression analysis is given below.

Table S2. Variable-energy data statistics for 1.

Energy (eV, uncalibrated)	No. reflections (total)	No. reflections (unique)	Data per frame	$wR_2(\text{int})$	$I/\sigma$ (limiting)	Resolution ( $\theta$ )
8910	5684	2646	15.92	0.0361	27.9	34.25
8915	11350	2647	15.9	0.0325	34.2	34.23
8920	11410	2663	16.03	0.0327	39.6	34.21
8925	5723	2667	16.08	0.0356	31.6	34.03
8930	11518	2680	16.18	0.0336	36.3	34.17
8935	11542	2680	16.21	0.034	37.7	34.15
8940	11536	2682	16.2	0.0344	34.3	34.13
8945	11546	2685	16.17	0.0349	35.8	34.1
8950	11564	2685	16.2	0.0355	34.4	32.15
8952	11562	2686	16.24	0.036	41	33.92
8954	11538	2684	16.21	0.0347	40.3	33.91
8956	11560	2687	16.24	0.0354	36.5	33.9
8958	11538	2682	16.21	0.0345	39.7	33.89
8960	11654	2687	16.28	0.0334	40.1	32.11
8962	11596	2695	16.29	0.0356	37.6	33.87

8964	11606	2699	16.25	0.0347	37.3	33.87
8966	17415	2702	16.31	0.0336	43.1	33.86
8968	11618	2704	16.27	0.0347	41.6	32.08
8970	11734	2697	16.39	0.0336	44.8	33.84
8972	5876	2705	16.41	0.0357	40.2	33.83
8974	11766	2711	16.43	0.0335	41.2	33.83
8976	5823	2708	16.31	0.0386	33.9	33.82
8978	17697	2719	16.48	0.0343	41.9	31.78
8980	11812	2727	16.5	0.0339	43.3	34.17
8982	11650	2707	16.32	0.0352	37.3	34.16
8984	11662	2710	16.33	0.0365	37.1	34.15
8986	11864	2732	16.57	0.038	36.2	34.15
8988	11862	2726	16.57	0.0388	37	31.97
8990	11864	2727	16.57	0.0401	35.5	34.13

Table S3. Variable-energy data statistics for 2.

Energy (eV, uncalibrated)	No. reflections (total)	No. reflections (unique)	Data per frame	wR <sub>2</sub> (int)	I/σ (limiting)	Resolution (θ)
8930	52330	2328	14.7	0.0306	32.3	31.84
8935	53460	2366	14.93	0.0305	30	31.82
8940	54140	2391	15.12	0.0317	29.1	32.05
8945	53640	2375	14.98	0.0316	31.7	32.03
8950	53880	2386	15.09	0.0325	31.2	32.01
8955	53960	2386	15.11	0.0326	33.1	31.99
8960	54080	2392	15.19	0.0335	31.9	31.97
8965	54640	2410	15.22	0.0344	28.8	31.94
8970	54150	2398	15.17	0.032	33.1	31.91
8972	54150	2398	15.17	0.032	33.7	31.91
8974	54170	2400	15.13	0.0318	31.3	31.9
8976	54300	2406	15.21	0.0317	31.1	31.89
8978	54360	2410	15.23	0.0319	33.1	31.88
8980	54250	2408	15.24	0.0308	31.9	31.88
8982	54250	2410	15.2	0.0312	34	31.87
8984	54220	2409	15.19	0.0315	33.2	31.86
8986	53990	2400	15.12	0.0333	32	31.84
8988	54287	2412	15.21	0.0365	27.5	31.84
8990	54460	2419	15.25	0.0534	20.5	31.83
8992	59774	2411	15.18	0.0447	22.4	31.82
8994	55460	2447	15.49	0.045	23.4	31.14
8996	55100	2445	15.39	0.0481	21.2	31.58

8998	54520	2423	15.27	0.0501	20.1	31.58
9000	55143	2444	15.36	0.0501	20.9	31.8
9003	55270	2451	15.48	0.0523	19.8	31.78
9006	49824	2451	15.46	0.0519	20.2	31.54
9009	55430	2456	15.48	0.0524	19.2	30.77
9015	55990	2474	15.64	0.0559	17.8	30.44
9018	56110	2476	15.67	0.0572	16.7	30.3
9021	56190	2479	15.65	0.0576	16.6	30.29
9024	56290	2479	15.68	0.056	17.8	30.21
9027	56200	2476	15.74	0.0573	17.6	30.2
9030	56350	2481	15.78	0.0575	18.6	30.19
9033	56510	2483	15.78	0.0583	18.8	30.18
9036	56550	2484	15.8	0.058	18.2	30.16
9039	5684	2490	15.88	0.06	15.1	30.15

Table S4. Variable-energy data statistics for **3**.

<b>Energy (eV, uncalibrated)</b>	<b>No. reflections (total)</b>	<b>No. reflections (unique)</b>	<b>Data per frame</b>	<b>wR<sub>2</sub>(int)</b>	<b>I/<math>\sigma</math> (limiting)</b>	<b>Resolution (<math>\theta</math>)</b>
8960	5919	2283	16.67	0.0598	15.4	33.45
8965	5928	2287	16.75	0.0606	14.8	33.43
8970	5941	2290	16.74	0.0658	13.8	33.41
8973	5935	2293	16.67	0.0593	15.6	33.02
8977	5949	2300	16.76	0.0605	15.6	33
8979	5959	2302	16.83	0.0613	18.1	31.06
8981	5962	2304	16.84	0.0622	17.7	31.05
8983	5966	2308	16.76	0.0617	16.6	31.04
8985	5966	2310	16.81	0.0609	18.5	31.04
8987	5963	2311	16.89	0.0614	18	31.03
8988	5969	2312	16.91	0.0616	20.1	31.02
8989	5966	2314	16.9	0.0626	17.3	31.02
8991	5974	2316	16.88	0.06	17.7	31.01
8992	5980	2321	16.85	0.0696	14	31.01
8994	5982	2319	16.9	0.0604	20.3	31
8995	5985	2322	16.86	0.0619	16.5	31
8996	5986	2322	16.96	0.0623	18.9	30.99
8997	5989	2324	16.82	0.0621	17.8	30.99
8998	5985	2325	16.95	0.0609	18.3	30.98
9000	5997	2328	16.94	0.0647	15.5	32.06
9001	11982	2331	16.92	0.0688	17	32.91
9003	5987	2322	16.91	0.0581	16.9	33.48

9006	5989	2324	16.87	0.0564	17.2	32.88
9009	6004	2327	16.91	0.0584	16.2	32.87
9014	6019	2335	17	0.0576	16.3	32.85
9019	6031	2338	17.04	0.0575	16.1	32.82
9024	6046	2342	17.08	0.0574	17.5	33.38
9029	6060	2344	17.07	0.0598	15.6	33.36

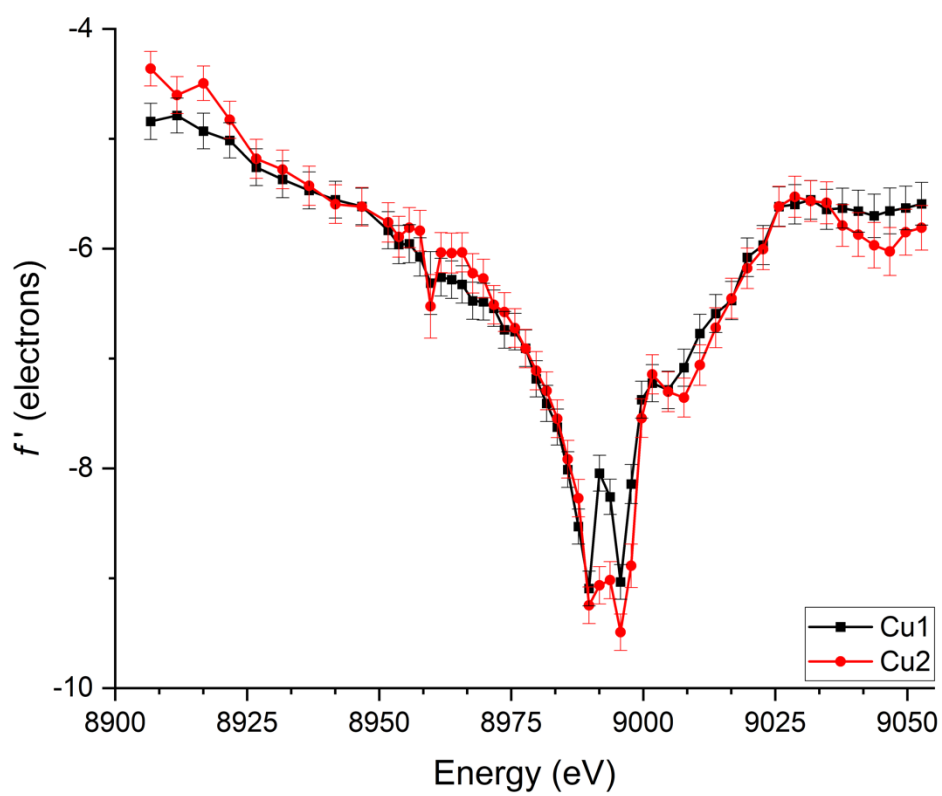


Figure S3. Plot of  $f'$  vs. energy for the two unique Cu sites in **1**, with error bars shown. Error bars were omitted in the main paper for clarity.

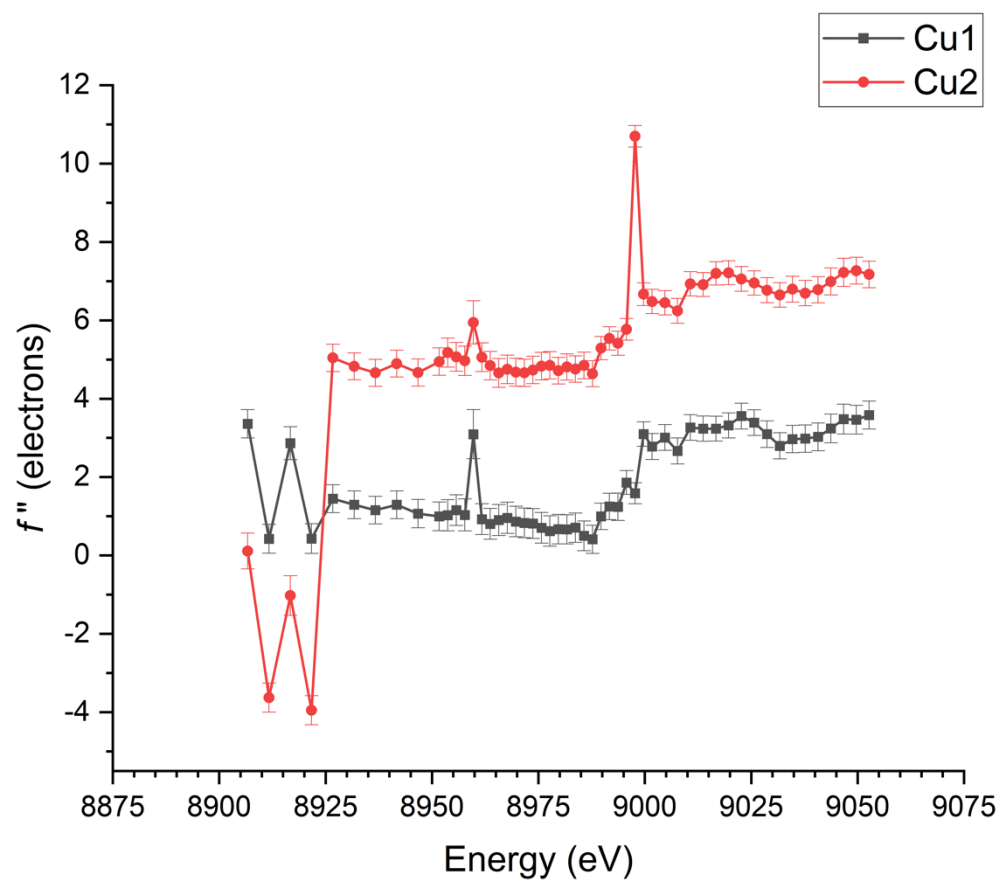


Figure S4. Plot of  $f''$  vs. energy for the two unique Cu sites in **1**.

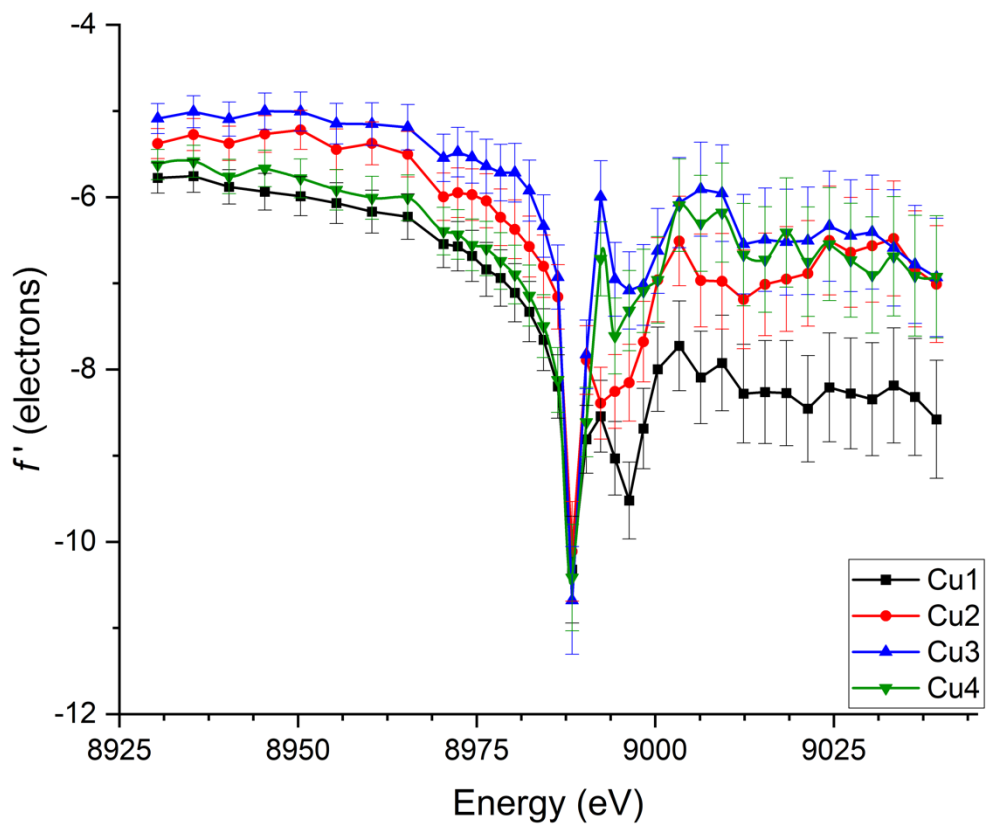


Figure S5. Plot of  $f'$  vs. energy for the four unique Cu sites in **2** with error bars shown. Error bars were omitted in the main paper for clarity.

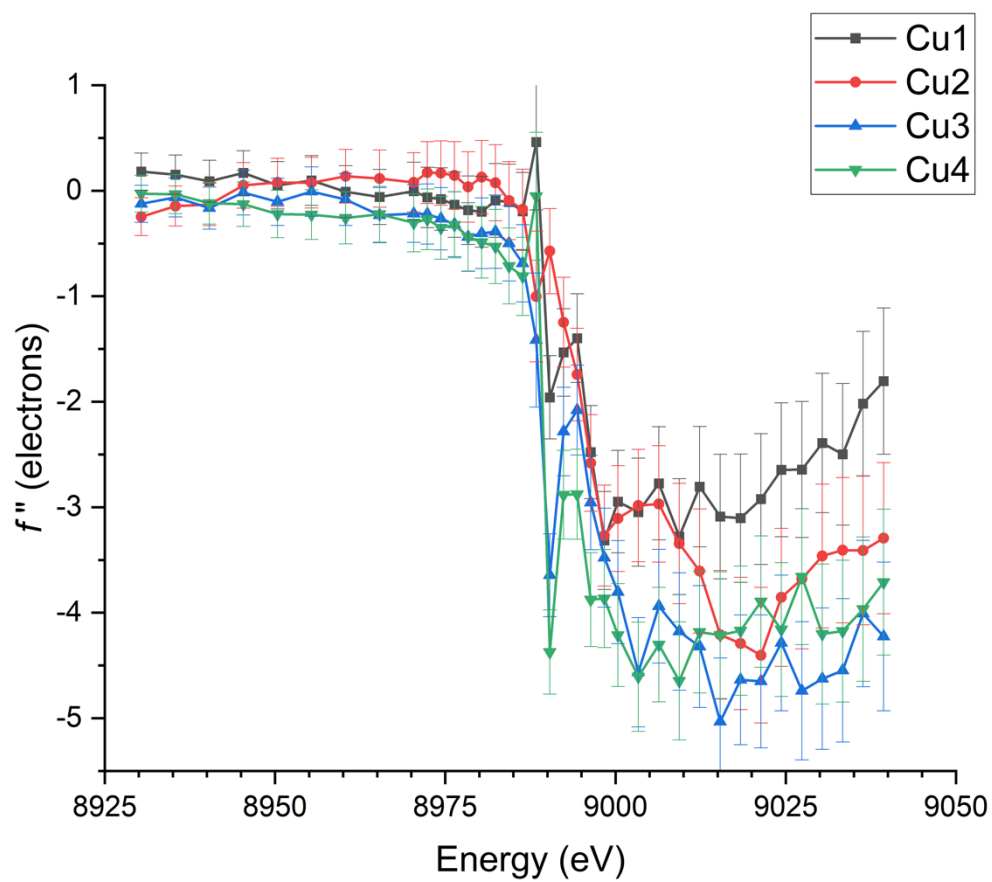


Figure S6. Plot of  $f''$  vs. energy for the four unique Cu sites in **2**.

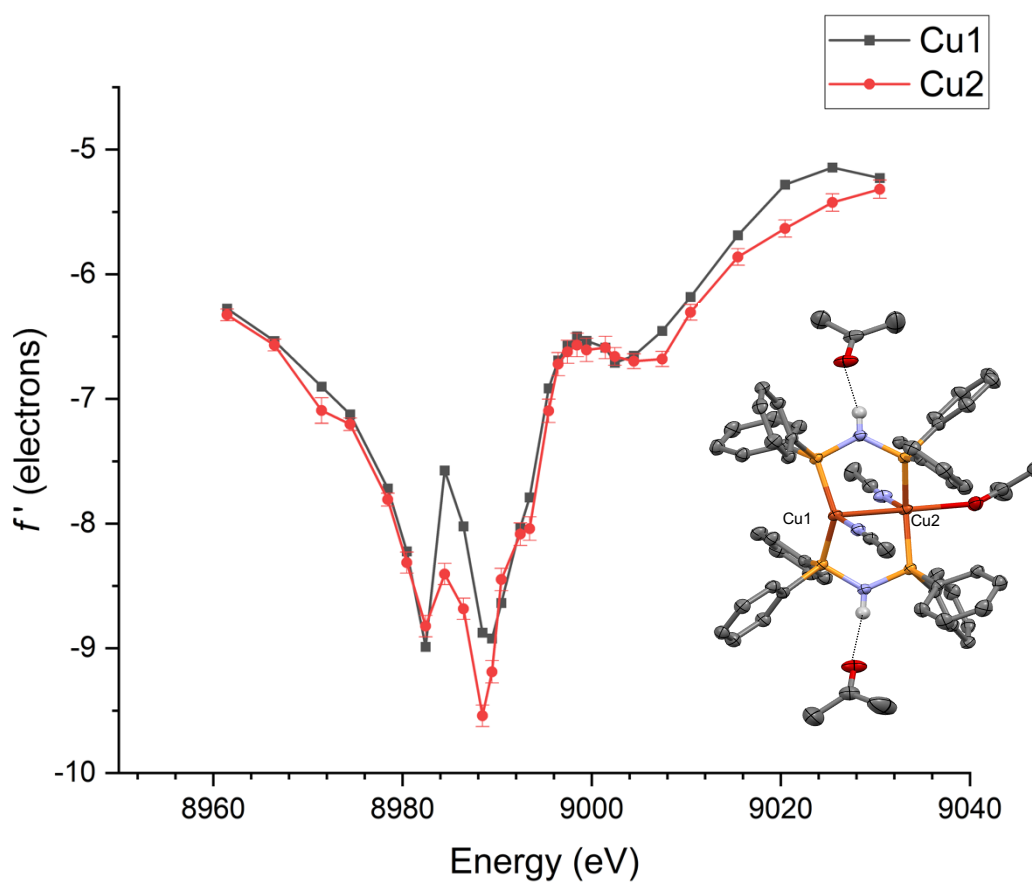


Figure S7. Plot of  $f'$  vs. energy for the two unique Cu sites in **3**, along with its crystal structure. Errors bars, which were omitted for clarity in the main paper, are shown here.

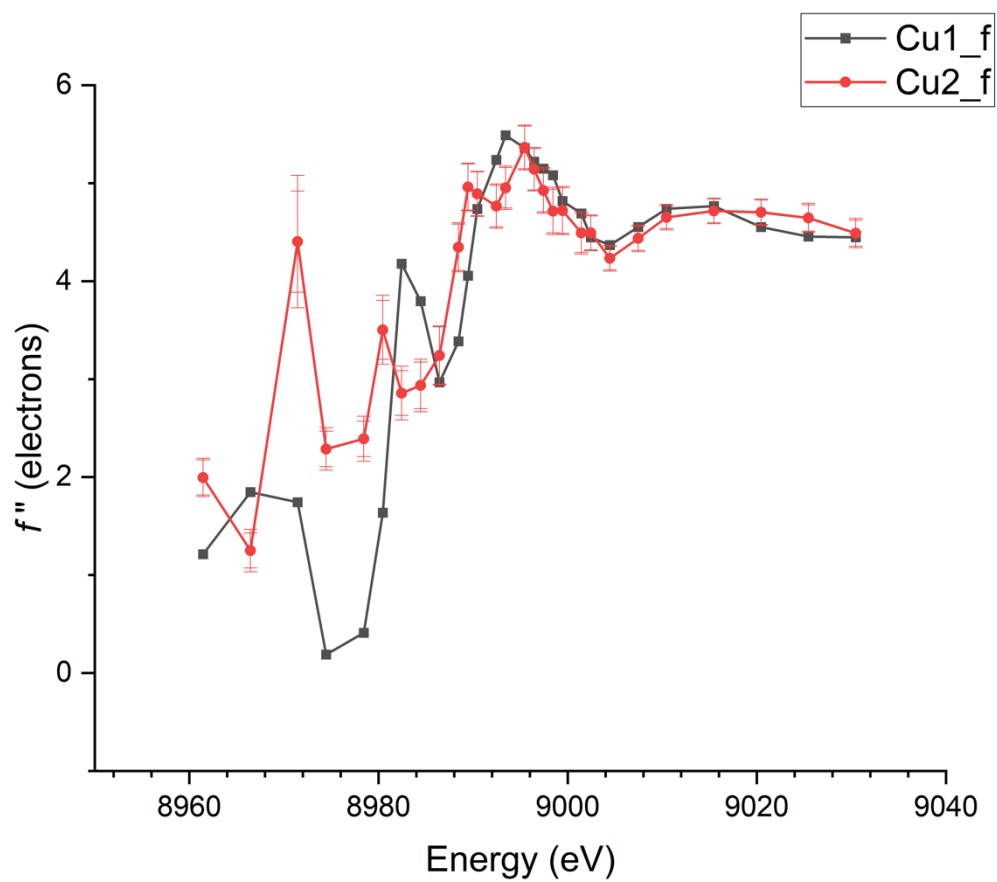


Figure S8. Plot of  $f''$  vs. energy for the two unique Cu sites in **3**.

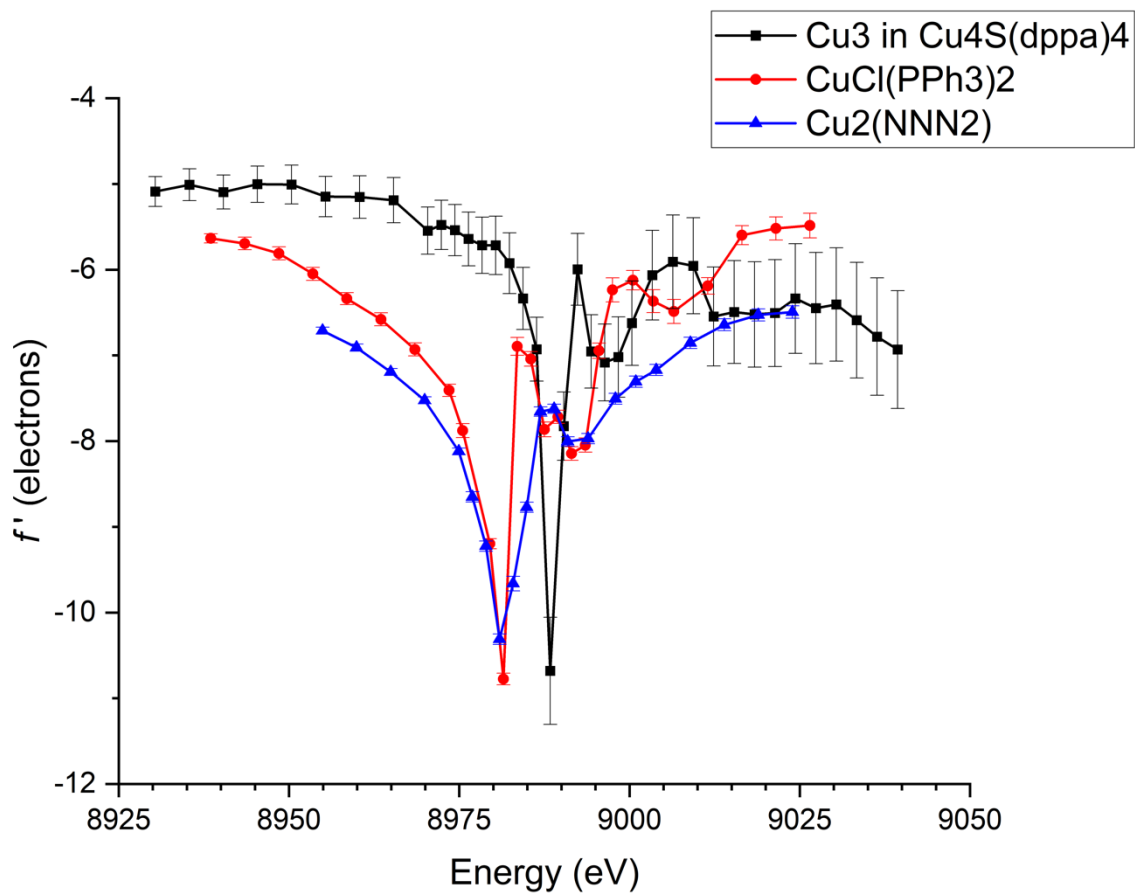


Figure S9. Comparison of the DAFS response for the  $\text{Cu}_3$  site in **2** with previously characterized complexes with three-coordinate Cu centers. Reference data were taken from Alayoglu et al.<sup>12</sup>

## Linear Regression Analysis of Rising-Edge Energies

From each DAFS data set (i.e.  $f'$  vs.  $E$  plot), data points were extracted from the “vertical” rising edge just to the right of the complex in-edge fine structure and fit to a line (Figure S10). Based on these linear fits, each complex’s energy values at  $f' = -7, -7.5, -8.5,$  and  $-9.5$  were interpolated. Data in the main paper come from interpolation at  $f' = -7.5$ , and the remaining data are shown in Table S2.

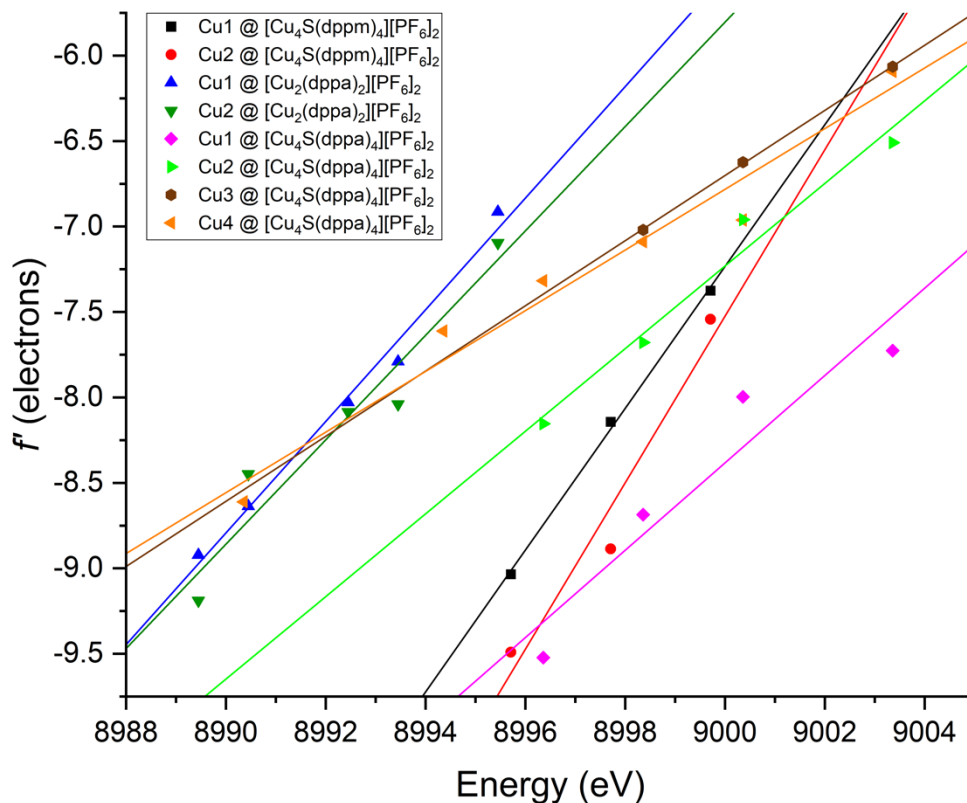


Figure S10. Linear fitting of Rising-Edge Energies.

Table S5. Interpolation of each complex's energy values from the linear fitting

Cu sites	$f' = -7$	$f' = -8.5$	$f' = -9.5$
<b>[Cu<sub>4</sub>S(dppm)<sub>4</sub>][PF<sub>6</sub>]<sub>2</sub> (1)</b>			
Cu1	9000.24	8996.63	8994.21
Cu2	9000.62	8997.53	8995.48
<b>[Cu<sub>4</sub>S(dppa)<sub>4</sub>][PF<sub>6</sub>]<sub>2</sub> (2)</b>			
Cu1	9006.26	9000.39	8996.48
Cu2	8998.15	8991.95	8987.81
Cu3	9004.02	8996.15	8990.91
Cu4	8998.32	8989.47	8983.62
<b>[Cu<sub>2</sub>(dppa)<sub>2</sub>][PF<sub>6</sub>]<sub>2</sub> (3)</b>			
Cu1	8995.82	8990.60	8987.11
Cu2	8996.99	8991.36	8987.60

## Computational Details

All DFT (density functional theory) calculations were performed using Gaussian 16 (Revision B.01).<sup>13</sup> The geometries were optimized with no constraints on symmetry utilizing the B3LYP functional using an ultrafine integration grid. The LANL2TZ basis set was used for Cu, and 6-31+G(d,p) was used for all other atoms. The solvent effects were taken into account using the SMD solvation model with default methanol parameters.<sup>14</sup> Vibrational frequency analysis confirmed that all stationary points were correctly identified as true potential energy surface minima with zero imaginary frequencies (stable intermediates). In one case (N<sub>2</sub>O binding along the Cu3-Cu4 edge), the optimized structure was calculated to have one imaginary frequency and, therefore, represents a transition state structure. Optimized geometries were visualized using CYLview20.<sup>15</sup> The optimized coordinates have been uploaded as Supporting Information in XYZ format. Partial atomic charge calculations were carried out using the open-source MultiWFN program<sup>16</sup> and the results are summarized in Table S3.

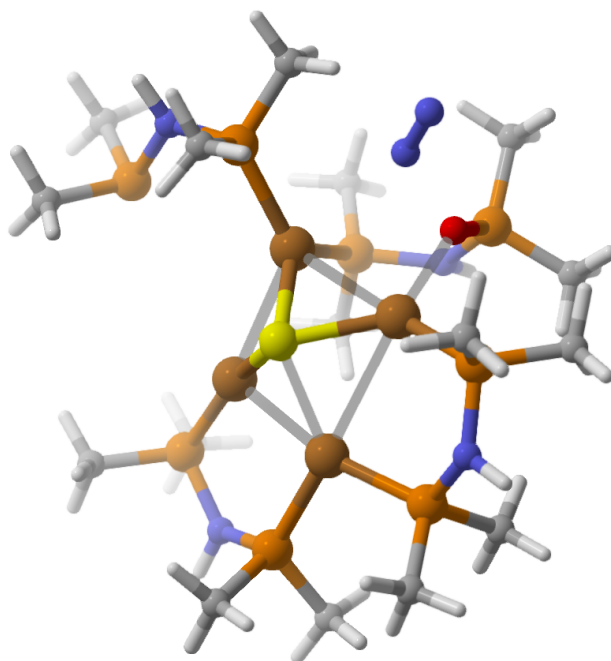


Figure S11. Energy minimized structure from N<sub>2</sub>O approach to **2** along the Cu1···Cu3 edge.

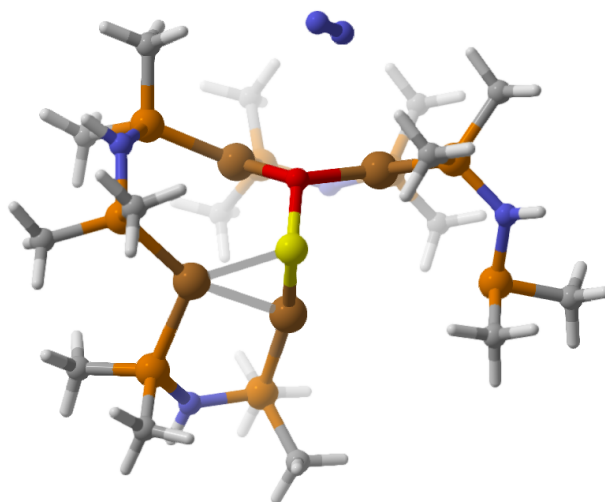


Figure S12. Energy minimized structure from N<sub>2</sub>O approach to **2** along the Cu3···Cu4 edge.

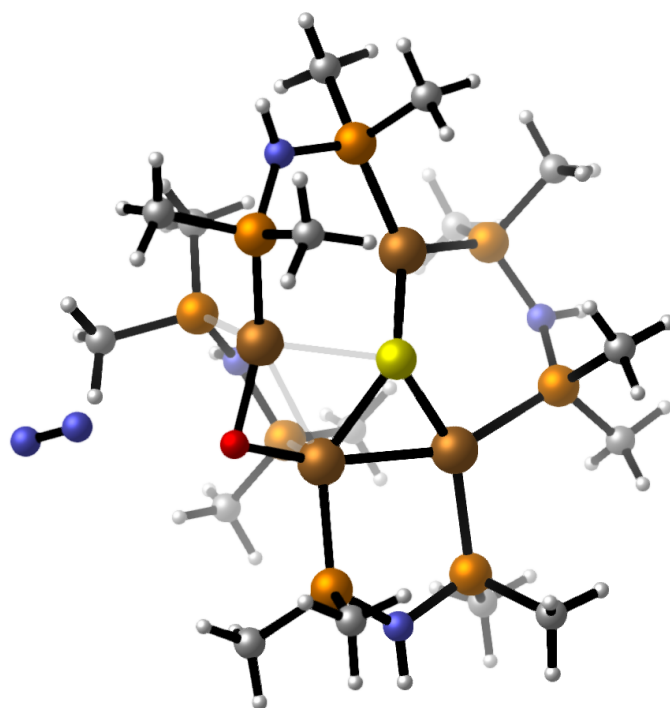


Figure S13. Energy minimized structure from N<sub>2</sub>O approach to **2** along the Cu2···Cu4 edge.

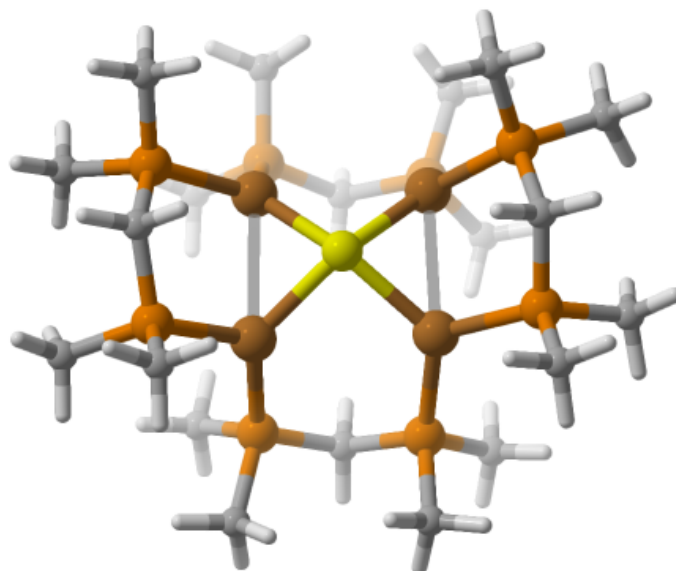


Figure S14. Energy minimized structure for a model of **1** with  $\text{PMe}_2$  groups in place of  $\text{PPh}_2$  groups.

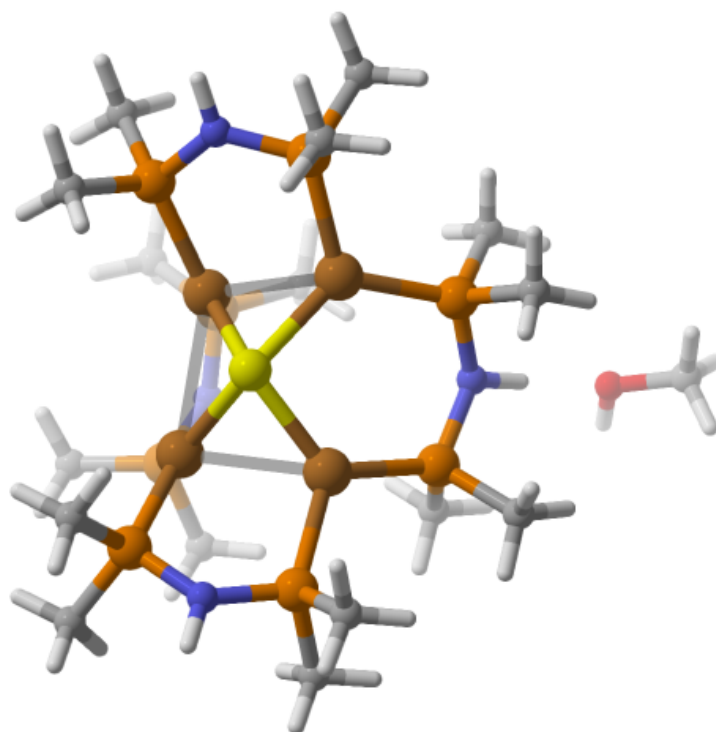


Figure S15. Energy minimized structure for a model of **2** with  $\text{PMe}_2$  groups in place of  $\text{PPh}_2$  groups, and with one explicit MeOH molecule engaged in hydrogen bonding.

Table S6. Partial atomic charge calculations for the truncated models of complexes **1** and **2**

	Hirshfeld charge	CM5 charge
<b>Complex 1</b>		
Cu1	0.162	0.358
Cu2	0.164	0.362
<b>Complex 2</b>		
Cu1	0.267	0.470
Cu2	0.155	0.357
Cu3	0.164	0.365
Cu4	0.138	0.342

## References

1. Pangborn, A. B., Giardello, M. A., Grubbs, R. H., Rosen, R. K. & Timmers, F. J. Safe and Convenient Procedure for Solvent Purification. *Organometallics* **15**, 1518–1520 (1996).
2. Yam, V. W. W., Lee, W. K. & Lai, T. F. Synthesis and luminescent properties of a novel tetranuclear copper(I) cluster containing a  $\mu_4$ -sulfur moiety. X-Ray crystal structure of  $[\text{Cu}_4(\mu\text{-dppm})_4(\mu_4\text{-S})](\text{PF}_6)_2 \cdot 2\text{Me}_2\text{CO}$  [dppm = bis(diphenylphosphino)methane]. *J. Chem. Soc. Chem. Commun.* **4**, 1571–1573 (1993).
3. Johnson, B. J., Lindeman, S. V. & Mankad, N. P. Assembly, structure, and reactivity of  $\text{Cu}_4\text{S}$  and  $\text{Cu}_3\text{S}$  models for the nitrous oxide reductase active site,  $\text{Cu}_Z$ . *Inorg. Chem.* **53**, 10611–10619 (2014).
4. Liu, H. *et al.* New Cu(I) and Ag(I) binuclear complexes containing the dppa ligand. *J. Chem. Soc. Dalton Trans.* 4365–4374 (2002) doi:10.1039/B205922N.
5. Sheldrick, G. M. A short history of SHELX. *Acta Crystallogr. A* **64**, 112–122 (2008).
6. Müller, P. Practical suggestions for better crystal structures. *Crystallogr. Rev.* **15**, 57–83 (2009).
7. Dolomanov, O. V., Bourhis, L. J., Gildea, R. J., Howard, J. A. K. & Puschmann, H. OLEX2 : a complete structure solution, refinement and analysis program. *J. Appl. Crystallogr.* **42**, 339–341 (2009).
8. Petříček, V., Dušek, M. & Palatinus, L. Crystallographic Computing System JANA2006: General features. *Z. Für Krist. - Cryst. Mater.* **229**, 345–352 (2014).
9. Bartholomew, A. K. *et al.* Exposing the inadequacy of redox formalisms by resolving redox inequivalence within isovalent clusters. *Proc. Natl. Acad. Sci.* **116**, 15836–15841 (2019).
10. Bartholomew, A. K. *et al.* Revealing redox isomerism in trichromium imides by anomalous diffraction. *Chem. Sci.* **12**, 15739–15749 (2021).
11. Ravel, B. & Newville, M. ATHENA , ARTEMIS , HEPHAESTUS : data analysis for X-ray absorption spectroscopy using IFEFFIT. *J. Synchrotron Radiat.* **12**, 537–541 (2005).

12. Alayoglu, P. *et al.* Metal Site-Specific Electrostatic Field Effects on a Tricopper(I) Cluster Probed by Resonant Diffraction Anomalous Fine Structure (DAFS). Preprint at <https://doi.org/10.26434/chemrxiv-2023-h1dxg> (2023).
13. Ortiz, J. V., Cioslowski, J. & Fox, D. J. Gaussian 09, revision B. 01. *Wallingford CT* (2009).
14. Marenich, A. V., Cramer, C. J. & Truhlar, D. G. Universal Solvation Model Based on Solute Electron Density and on a Continuum Model of the Solvent Defined by the Bulk Dielectric Constant and Atomic Surface Tensions. *J. Phys. Chem. B* **113**, 6378–6396 (2009).
15. Legault, C. Y. CYLview20. (2020).
16. Lu, T. & Chen, F. Multiwfn: A multifunctional wavefunction analyzer. *J. Comput. Chem.* **33**, 580–592 (2012).